Doping evolution of the superconducting gap structure in the underdoped iron arsenide $Ba_{1-x}K_{x}Fe_{2}As_{2}$ revealed by thermal conductivity

J.-Ph. Reid, M. A. Tanatar, X. G. Luo, H. Shakeripour, S. René de Cotret, A. Juneau-Fecteau, J. Chang, B. Shen, H.-H. Wen, H. Kim, R. Prozorov, N. Doiron-Leyraud, and Louis Taillefer

Phys. Rev. B **93**, 214519 — Published 30 June 2016

DOI: 10.1103/PhysRevB.93.214519

Doping evolution of the superconducting gap structure in the underdoped iron arsenide $Ba_{1-x}K_xFe_2As_2$ revealed by thermal conductivity

J.-Ph. Reid,[1] M. A. Tanatar,[2] X. G. Luo,[1] H. Shakeripour,[1,3] S. René de Cotret,[1] A. Juneau-Fecteau,[1] J. Chang,[1] B. Shen,[4] H.-H. Wen,[4,5] H. Kim,[2,6] R. Prozorov,[2,6] N. Doiron-Leyraud,[1] and Louis Taillefer[1,5,*]

[1]*Département de physique & RQMP, Université de Sherbrooke, Sherbrooke, Québec J1K 2R1, Canada*
[2]*Ames Laboratory, Ames, Iowa 50011, USA*
[3]*Department of Physics, Isfahan University of Technology, Isfahan 84156-83111, Iran*
[4]*Center for Superconducting Physics and Materials, National Laboratory of Solid State Microstructures and Department of Physics, Nanjing University, Nanjing 210093, China*
[5]*Canadian Institute for Advanced Research, Toronto, Ontario M5G 1Z8, Canada*
[6]*Department of Physics and Astronomy, Iowa State University, Ames, Iowa 50011, USA*

(Dated: May 9, 2016)

The thermal conductivity κ of the iron-arsenide superconductor $Ba_{1-x}K_xFe_2As_2$ was measured for heat currents parallel and perpendicular to the tetragonal c axis at temperatures down to 50 mK and in magnetic fields up to 15 T. Measurements were performed on samples with compositions ranging from optimal doping ($x = 0.34$; $T_c = 39$ K) down to dopings deep into the region where antiferromagnetic order coexists with superconductivity ($x = 0.16$; $T_c = 7$ K). In zero field, there is no residual linear term in $\kappa(T)$ as $T \to 0$ at any doping, whether for in-plane or inter-plane transport. This shows that there are no nodes in the superconducting gap. However, as x decreases into the range of coexistence with antiferromagnetism, the residual linear term grows more and more rapidly with applied magnetic field. This shows that the superconducting energy gap develops minima at certain locations on the Fermi surface and these minima deepen with decreasing x. We propose that the minima in the gap structure arise when the Fermi surface of $Ba_{1-x}K_xFe_2As_2$ is reconstructed by the antiferromagnetic order.

PACS numbers: 74.25.Fc, 74.20.Rp, 74.70.Xa

I. INTRODUCTION

Soon after the discovery of superconductivity in iron-based materials,[1] it was recognized that a conventional phonon-mediated pairing cannot account for the high critical temperature T_c.[2] The observation of superconductivity in proximity to a magnetic quantum critical point[3] points instead to magnetically-mediated pairing,[4] a scenario also discussed for cuprate and heavy-fermion materials.[5] Because such pairing is based on a repulsive interaction, it implies that the superconducting order parameter must change sign around the Fermi surface.[6] This is the case for the d-wave state realized in cuprate superconductors, where the gap has symmetry-imposed nodes where the Fermi surface crosses the diagonals at $k_x = k_y$. In the $s_\pm$ state proposed for iron-based superconductors,[7] there are no symmetry-imposed nodes, but the order parameter has a different sign on the hole and electron pockets. One can see that in order to identify the pairing symmetry, associated with a particular pairing mechanism, it is important to determine the anisotropy of the gap structure.

In the iron-based superconductors, the superconducting gap structure has been studied most extensively in the oxygen-free materials with $BaFe_2As_2$ (Ba122) as a parent compound.[8] High-quality single crystals can be grown with various types of dopants to induce superconductivity in the parent antiferromagnet, including: hole doping with potassium in $Ba_{1-x}K_xFe_2As_2$ (K-Ba122),[9] electron doping with cobalt in $Ba(Fe_{1-x}Co_x)_2As_2$ (Co-Ba122),[10,11] and iso-electron substitution of arsenic with phosphorus in $BaFe_2(As_{1-x}P_x)_2$ (P-Ba122).[12]

Early on, an ARPES study of optimally-doped K-Ba122 found a full superconducting gap on all sheets of the Fermi surface.[13] This was explained within the $s_\pm$ scenario.[14] However, subsequent studies of the superconducting gap structure in Ba122 revealed considerable diversity. In P-Ba122, the gap is nodal for all dopings.[15,16] In Co-Ba122, the gap is isotropic at optimal doping but it develops nodes in both under- and over-doped compositions.[17–21] In K-Ba122, the gap is also isotropic at optimal doping,[13,22] but it develops some k-dependence with decreasing x,[23–26] and there are nodes in the gap at $x = 1.0$ (KFe_2As_2),[27–32] and close to x=1, where the pairing symmetry may in fact be d-wave.[22,30,33]

This diversity in the gap structure has been attributed in part to a competition between intra-band and inter-band pairing interactions.[34,35] Another factor that can affect the gap structure is the presence of a coexisting antiferromagnetic order.[36] The importance of the coexisting magnetism for the superconducting gap structure of hole-doped K-Ba122 was suggested by a previous penetration depth study,[25] which found a rapid loss of superfluid response on underdoping into the coexistence range. A similar decrease was observed in electron-doped Co-122.[37] In this Article, we report a study of the superconducting gap structure in K-Ba122 using directional heat transport measurements, for concentrations that cross into the region of the phase diagram where superconductivity and antiferromagnetism coexist. We observe that

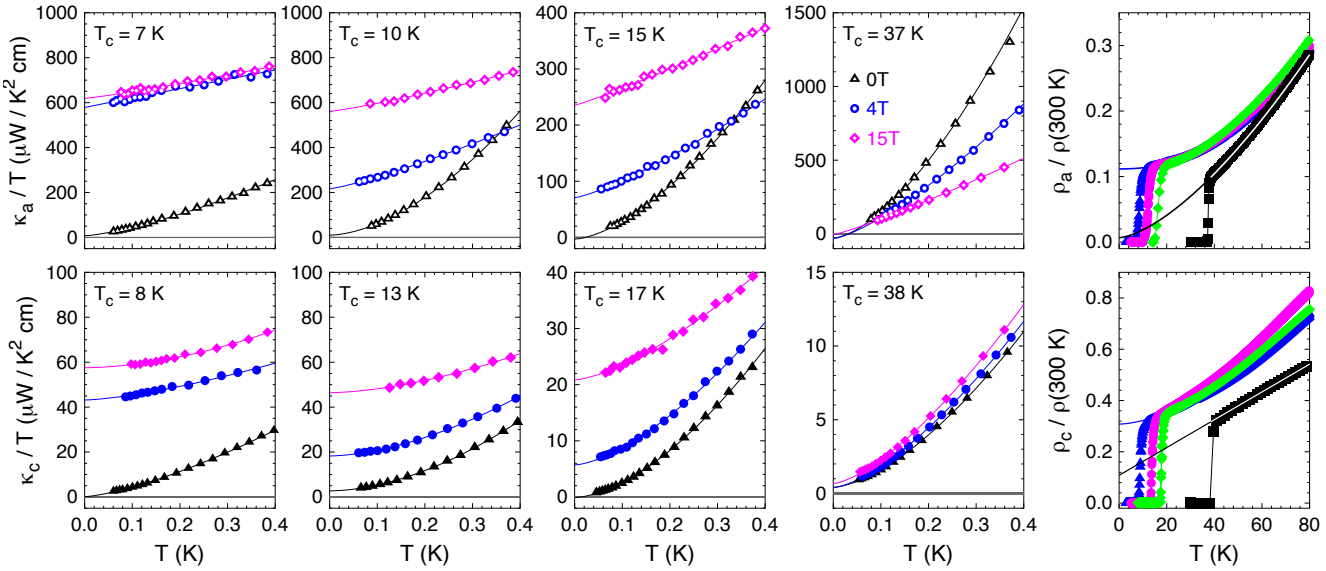

FIG. 1: Thermal conductivity of K-Ba122 at four representative K concentrations, indicated by their T_c values, plotted as κ/T vs T for in-plane (κ_a, top panels) and inter-plane (κ_c, bottom panels) directions of the heat current. Data are shown for three values of the magnetic field, as indicated (data for other fields are not shown for clarity). Lines are fits to $\kappa/T = a + bT^{\alpha}$, used to extract the residual linear term $a \equiv \kappa_0/T$. The right-most panels show the electrical resistivity of the same samples, normalized to its value at $T = 300$ K, as a function of temperature. The line is a fit to the data at low temperature, extended to $T = 0$ to extract the residual resistivity ρ_0. For clarity, only the fits for samples with $T_c \cong 7$ K and 38 K are shown.

the gap, which is isotropic just above the coexistence region, gradually develops k dependence as the magnetic order grows, with minima that deepen with decreasing x. We attribute these minima to the reconstruction of the Fermi surface caused by the antiferromagnetic order.

Our main findings may be summarised as follows. The superconducting gap of K-Ba122 does not have nodes for a broad range of under-doped compositions in the phase diagram, from $x = 0.16$ ($T_c = 7$ K) to $x = 0.34$ ($T_c = 39$ K). However, a notable modulation of the superconducting gap magnitude develops in the coexistence regime of superconductivity and magnetism ($x < 0.25$), as found in strongly enhanced response to application of magnetic field. The $a - c$ directional anisotropy of heat transport in the superconducting state of K-Ba122 is identical to the anisotropy of the normal state, suggesting that modulation of the superconducting energy gap is predominantly in the conducting plane, which is in sharp contrast to the electron-doped (Co-Ba122)[20].

II. METHODS

Single crystals of $Ba_{1-x}K_xFe_2As_2$ were grown using a self-flux technique.[9] Nine samples were cut for a-axis transport and seven for c-axis transport. The samples are labelled by their T_c value. Details of the sample preparation, screening, compositional analysis and resistivity measurements can be found in ref. 38. The technique for making contacts is described in refs. 39 and 40. The superconducting T_c of underdoped samples changes monotonically with x. We find that the relation between T_c and x is well described by the formula $T_c = 38.5 - 54\,(0.345 - x) - 690\,(0.345 - x)^2$. The thermal conductivity was measured in a standard one-heater two-thermometer technique described elsewhere,[20] for two directions of the heat flow: parallel ($Q \parallel c$; κ_c) and perpendicular ($Q \parallel a$; κ_a) to the [001] tetragonal c axis. The magnetic field H was applied along the c axis. Measurements were done on warming after cooling from above T_c in a constant field, to ensure a homogeneous field distribution in the sample. At least two samples were measured for all compositions to ensure reproducibility. Resistivity measurements to determine the upper critical field were performed in *Quantum Design* PPMS down to 1.8 K.

III. RESULTS

A. Electrical resistivity

In the right panels of Fig. 1, the resistivity of four K-Ba122 samples, normalized to its value at $T = 300$ K, is plotted as a function of temperature, for both $J \parallel a$ and $J \parallel c$. The values at 300 K, $\rho(300\text{ K})$, do not change much with doping, and $\rho(300\text{ K}) \simeq 300$ and 1000-2000 $\mu\Omega$ cm, respectively.[38,41] We use the resistivity curves of each sample to determine T_c and the residual resistivity ρ_0, obtained from a smooth extrapolation of $\rho(T)$ to $T = 0$

(see Fig. 1). We use ρ_0 to estimate the residual value of the thermal conductivity in the normal state, κ_N/T, via the Wiedemann-Franz law, $\kappa_N/T = L_0/\rho_0$, where $L_0 \equiv (\pi^2/3)(k_B/e)^2$.

B. Thermal conductivity

The thermal conductivity of the same four samples, measured using the same contacts, is also displayed in Fig. 1. The data in the top row are for a heat current along the a axis, giving κ_a, while the data in the bottom panels are for the inter-plane heat current, giving κ_c. The fits show that the data below 0.3 K are well described by the power-law function $\kappa/T = a + bT^\alpha$. The first term, $a \equiv \kappa_0/T$, is the residual linear term, entirely due to electronic excitations.[42] The second term is due to phonons, which at low temperature are scattered by the sample boundaries, with $1 < \alpha < 2$.[46,47] We see that for $H = 0$, $\kappa_0/T = 0$ for all samples, within error bars. At the highest doping ($T_c = 37 - 38$ K), κ_0/T remains negligible even when a magnetic field of 15 T is applied. At lower K concentration, however, κ_0/T increases significantly upon application of a magnetic field. Our current data are consistent with our previous measurement of κ_a in a K-Ba122 sample with $T_c = 26$ K.[23]

Fig. 2 shows how the residual linear term κ_0/T evolves as a function of magnetic field H, for both in-plane (top panel) and inter-plane (bottom panel) heat current directions. In this Figure, κ_0/T is normalized by the sample's normal-state conductivity, κ_N/T, and the magnetic field is normalized by the sample's upper critical field H_{c2} (determined as described in the next section). In Fig. 4, the ratio $(\kappa_0/T)\,/\,(\kappa_N/T)$ is plotted as a function of K concentration x, for two values of the magnetic field: $H = 0$ and $H = 0.15\ H_{c2}$.

C. Upper critical field

In the left panel of Fig. 3, we plot the upper critical field H_{c2} as a function of temperature, for four values of x, as determined from resistivity measurements for $H \parallel c$. For the sample at $x = 0.16$ ($T_c = 7$ K), a field of 15 T is sufficient to reach the normal state. Using the fact that κ_0/T saturates above $H \simeq 9$ T in that sample, we estimate that $H_{c2} = 9$ T at $T \to 0$. We see that this value agrees with a linear extrapolation of the resistively-determined $H_{c2}(T)$. For the other dopings, we obtain $H_{c2}(0)$, the value of $H_{c2}(T)$ at $T \to 0$, by linear extrapolation. Note that the slope of the $H_{c2}(T)$ curves increases with increasing T_c, as expected for superconductors in the clean limit,[41] which holds for K-Ba122 at all dopings. In the right panel of Fig. 3, we plot $H_{c2}(0)$ vs T_c, including published data from a sample with a slightly higher concentration.[41]

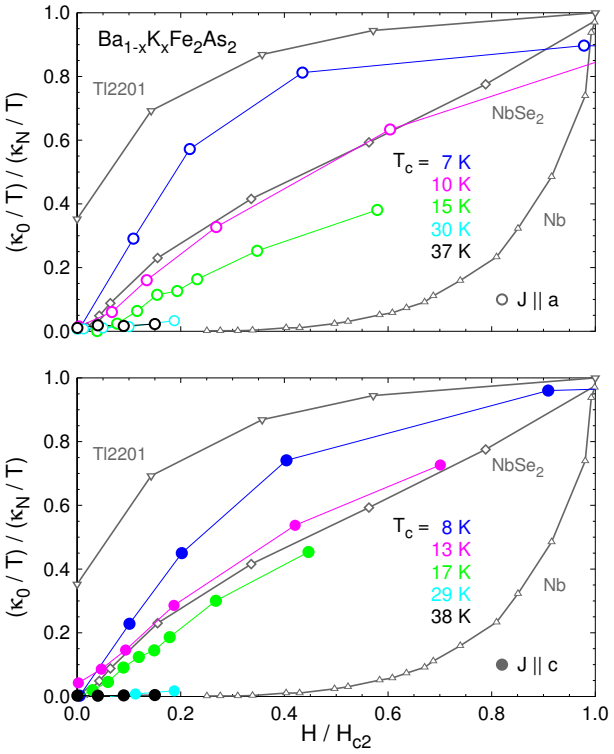

FIG. 2: Residual linear term κ_0/T, normalized by the normal-state conductivity, κ_N/T, as a function of magnetic field H, normalized by the upper critical field H_{c2} (defined in Fig. 3). The data for in-plane ($J \parallel a$, open symbols) and inter-plane ($J \parallel c$, closed symbols) transport are shown for five K concentrations, indicated by their T_c values. For comparison, we reproduce corresponding data for the isotropic s-wave superconductor Nb,[42,43], the multi-band s-wave superconductor $NbSe_2$,[44] and the nodal d-wave superconductor Tl-2201.[45]

IV. DISCUSSION

From Fig. 2, three main characteristics of the gap structure of K-Ba122 can be deduced. First, the fact that in zero field $\kappa_0/T = 0$ at all dopings, for both current directions, immediately implies that there are no zero-energy quasiparticles at $H = 0$. From this we can infer that there are no nodes in the superconducting gap anywhere on the Fermi surface.

Secondly, we see that the rate at which a magnetic field excites heat-carrying quasiparticles in K-Ba122 varies enormously with doping. In the absence of nodes, quasiparticle conduction proceeds by tunnelling between states localized in the cores of adjacent vortices, which grows exponentially as the inter-vortex separation decreases with increasing field,[44] as observed in a superconductor with an isotropic gap like Nb (see Fig. 2). The exponential rate is controlled by the coherence length, which is inversely proportional to the gap magnitude. If the gap is large everywhere on the Fermi surface, the coherence length will be small everywhere, and the

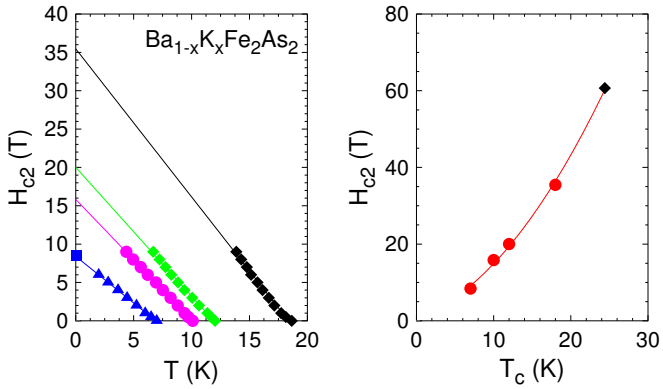

FIG. 3: Left panel: Upper critical field $H_{c2}(T)$ for $H \parallel c$, as a function of temperature, for four samples, with $T_c = 7$ (black), 10 (red), 12 (blue) and 19 K (green). H_{c2} is determined from electrical resistivity measurements.[41] The black square shows the H_{c2} value determined from thermal conductivity measurements on the $T_c = 7$ K sample. The lines are a linear fit of each data set, extrapolated to $T = 0$. The value of H_{c2} thus extrapolated to $T = 0$, $H_{c2}(0) \equiv H_{c2}$, is plotted vs x in the right panel. Right panel: $H_{c2}(0)$ vs T_c from data in the left panel (red dots), plus one point at high doping from published data (black diamond).[41] The line is a polynomial fit of the data, used to extract the values of H_{c2} for the samples with $T_c \in [7, 25]$ K.

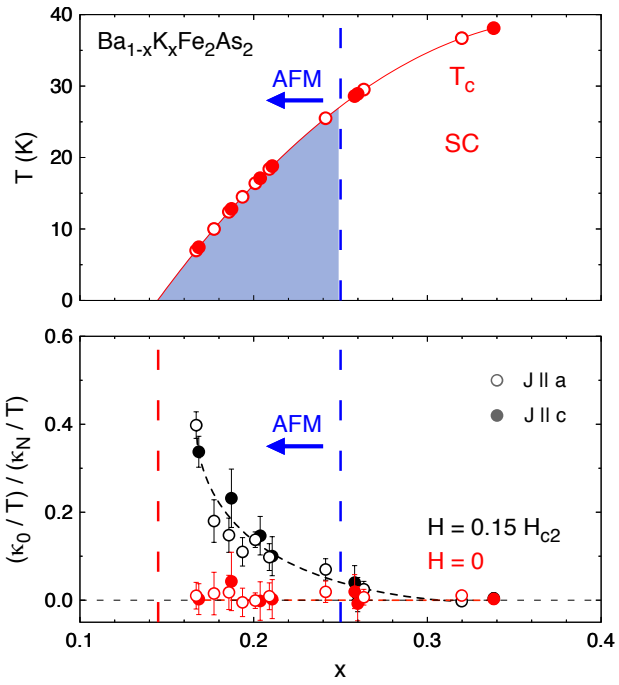

FIG. 4: Top panel: Doping phase diagram of K-Ba122, showing the onset of the superconducting phase (SC) below the critical temperature T_c as a function of the K concentration (doping) x. Open (closed) red circles give the T_c values of the a-axis (c-axis) samples used in this study. For compositions to the left of the dashed blue line at $x \simeq 0.25$ ($T_c \simeq 26$ K),[38,53] superconductivity coexists with antiferromagnetism (AFM). Bottom: Residual linear term in the thermal conductivity κ as $T \to 0$, κ_0/T, plotted as a fraction of the normal-state conductivity, κ_N/T, for both κ_a (open symbols) and κ_c (closed symbols), for magnetic fields $H = 0$ (red) and $H = 0.15\ H_{c2}$ (black). Error bars reflect the combined uncertainties of extrapolating κ/T and ρ to $T = 0$, to get κ_0/T and ρ_0. The red vertical dashed line at $x = 0.15$ marks the end of the superconducting phase.

growth of κ_0/κ_N vs H will be very slow at low H/H_{c2}. This is what we observe in K-Ba122 near optimal doping ($T_c \simeq 37$ K).

If the gap is small on some part of the Fermi surface, compared to the maximum value that dictates H_{c2}, this will make it easier to excite quasiparticles, and so lead to an enhanced thermal conductivity at a given value of H/H_{c2}. This is what happens in K-Ba122 with decreasing x, whereby κ_0/κ_N becomes larger and larger with underdoping. A good way to visualize this evolution is to plot κ_0/κ_N vs x at $H/H_{c2} = 0.15$, as done in Fig. 4. We infer from our in-field data that the gap structure of K-Ba122 develops a minimum somewhere on its Fermi surface, which gets deeper and deeper upon entering the coexisting antiferromagnetic phase. This is consistent with the behavior of the in-plane penetration depth,[25] which reveals a notable decrease of the superfluid stiffness in the coexistence range, and exhibits a transformation of its temperature dependence, $\Delta\lambda_a(T)$, from an exponential at optimal doping to a power-law with $n \approx 2$ at heavily underdoped compositions. This is a key signature of a gap structure with strong modulation, and possibly nodes, triggered by the onset of the long-range magnetic order. However, unlike our directional thermal conductivity measurements, penetration depth measurements cannot rule out the presence of accidental nodes in the gap structure.

There are two ways in which the gap can be small on part of the Fermi surface. It can develop a strong anisotropy on one sheet of the Fermi surface, as is believed to happen in borocarbide superconductors.[48] It can also be small on one surface and large on another. This multi-band scenario is what happens in MgB_2 (ref. 49) and $NbSe_2$ (ref. 44). In both cases, κ_0/κ_N grows fast, according to a field scale $H^\star$ much smaller than H_{c2}, as it is controlled by the minimum gap. See Fig. 2 for the data on $NbSe_2$.

The third property of the κ_0/κ_N vs H data in Fig. 2 is its isotropy with respect to current direction. The same behaviour is observed for in-plane and inter-plane heat currents. This implies that the minima which develop in the gap structure have no strong k_z dependence, *i.e.* they run vertically along the c axis.

In Fig. 5, we provide a sketch of how the superconducting gap structure evolves with doping in K-Ba122, in terms of a simple one-band Fermi surface. Since the gap modulation has no significant k_z dependence, we limit our discussion to a 2D picture. At high x, the gap is

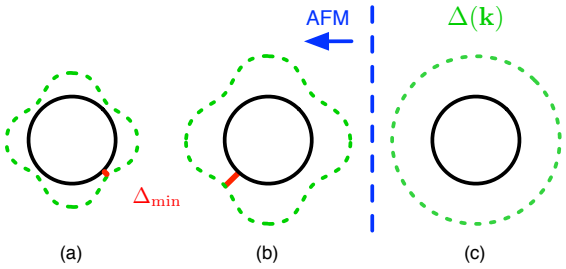

FIG. 5: Sketch of the evolution of the gap structure in K-Ba122 with doping x, where the gap (green dash line) is shown around a single Fermi surface (black circle). The gap is isotropic at optimal doping (c). The modulation of the gap starts upon entering the region where antiferromagnetism (AFM) appears, and coexists with superconductivity (panel b). The gap minimum deepens with decreasing x (panel a).

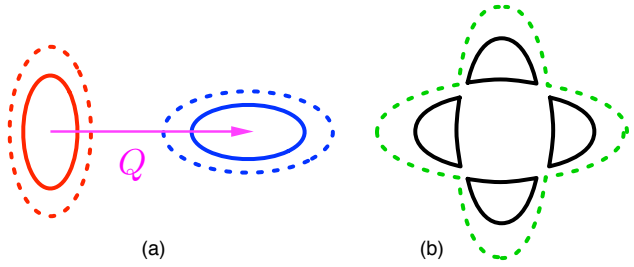

FIG. 6: (a) Sketch of the evolution of the superconducting gap structure (dashed line) in K-Ba122 as the Fermi surface (solid line) is reconstructed by antiferromagnetic order with a wave-vector $\mathbf{Q}$ as drawn.[36] (b) When the hole (red) and electron (blue) pockets overlap as a result of Fermi-surface reconstruction, an energy gap opens at the crossing points, and this leads to the formation of small crescent-like pieces. Calculations show that this can lead to the development of minima in the superconducting gap, or even nodes.[36]

isotropic (panel c), meaning that there is no indication of any modulation of the gap with angle. Upon lowering x, the gap acquires a modulation, with a minimum gap $\Delta_{\rm min}$ along some direction (panel b), and the gap minimum deepens with decreasing x (panel a). This explains why the initial rise in $\kappa_0/\kappa_{\rm N}$ vs H is gets steeper with decreasing x (Fig. 2).

The question is: why does the gap develop a modulation? In a number of calculations applied to pnictides, the so-called $s_\pm$ state is the most stable. This is a state with s-wave symmetry but with a gap that changes sign in going from the hole-like Fermi surface centred at Γ ($\Delta_h > 0$) to the electron-like Fermi surfaces centred at X and M ($\Delta_e < 0$).[50–52] Although fundamentally nodeless, the associated gap function can have strong modulations, depending on details of the Fermi surface and the interactions, possibly leading to accidental nodes.[35] The gap modulation comes from a strongly anisotropic pairing interaction, which is also band-dependent, involving the interplay of intra-band and inter-band interactions. It is typically the gap on the electron Fermi surface centred at the M point of the Brillouin zone that shows a strong angular dependence within the basal plane.[51,52] Therefore, the evolution of the gap structure detected here in K-Ba122, going from isotropic to modulated with decreasing x, is compatible with the general findings of such calculations. In Co-Ba122, the development of gap modulations with overdoping was attributed to such a change in interactions.[20]

We propose that another mechanism is at play on the underdoped side of the phase diagram, having to do with the onset of antiferromagnetic order. This is based on the fact that the modulation of the gap and the magnetic order appear at the same concentration, as seen in Fig. 4.

Neutron scattering studies show that antiferromagnetic order in K-Ba122 coexists with superconductivity over a broad range of doping, up to $x \simeq 0.25$ ($T_{\rm c} \simeq 26$ K), and both magnetism and superconductivity are bulk and occupy at least 95% of the sample volume.[53] (The fact that $\kappa_0/T = 0$ for $H = 0$ in all our samples rules out a scenario of phase separation, whereby significant portions of the sample are not superconducting.) This bulk coexistence is deemed to be a strong argument in favour of the $s_\pm$ model, and one against the usual s-wave scenario.[54,55]

Antiferromagnetism in K-Ba122 causes a reconstruction of the Fermi surface whereby the Γ-centered hole pocket becomes superpimposed on the edge-centered electron pocket, as sketched in Fig. 6. Energy gaps open at the points where the original two Fermi pockets cross, resulting in the formation of four small crescent-shaped pieces (Fig. 6). Maiti *et al.*[36] showed theoretically that such a reconstruction triggers a strong modulation of the superconducting gap, which develops strong minima, and possibly even (accidental) nodes, at the crossing points. It therefore seems natural to attribute the appearance of gap minima in underdoped K-Ba122 to the onset of magnetic order.

It is known that the orthorhombic distortion and the superconductivity are intimately coupled in KBa122.[56] It was shown theoretically that when both the superconducting and the orthorhombic order parameters are taken into account, the anisotropy of the superconducting coherence length can be greatly enhanced.[57] This could also explain the appearance of the gap anisotropy in this material.

In underdoped Co-Ba122, a similar thermal conductivity study revealed that a strong modulation of the gap also appears with the onset of magnetic order.[20] So the two materials tell a consistent story. In Fig. 7, we compare the evolution of the gap as found in thermal conductivity measurements on the two sides of the phase diagram of $BaFe_2As_2$: the electron-doped side (Co-Ba122) and the hole-doped side (K-Ba122). In both cases, the gap is isotropic close to optimal doping, and it develops a strong modulation with underdoping, concomitant with the onset of antiferromagnetism.

However, there is a difference between K-Ba122 and

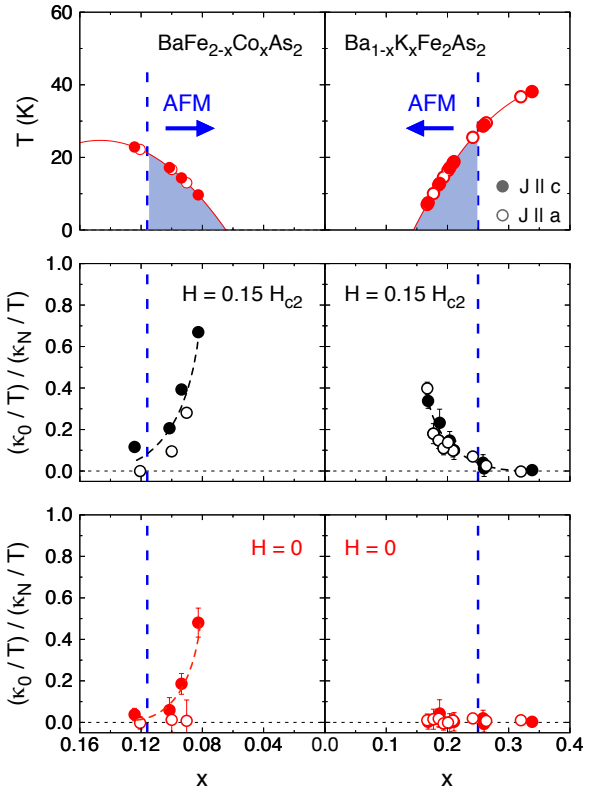

FIG. 7: Comparison of the superconducting gap anisotropy determined from thermal conductivity studies in electron-doped Co-Ba122 (left column)[19,20] and hole-doped K-Ba122 (right column, this work). The top panels show the phase diagrams of both materials. The middle and bottom panels show κ_0/κ_N vs x for $H = 0.15\ H_{c2}$ and $H = 0$, respectively. Open (closed) symbols correspond to transport along $J \parallel a$ ($J \parallel c$).

Co-Ba122. The former does not develop nodes, while the latter does. These nodes are in regions of the Fermi surface with strong k_z dispersion, as they give rise to a large zero-field value of κ_0/T for $J||c$, but not for $J||a$ (Fig. 7, bottom panel).[20]

V. SUMMARY

In summary, the thermal conductivity of K-Ba122 in the $T = 0$ limit reveals three main facts. First, the superconducting gap at optimal doping, where T_c is maximal, is isotropic, with no sign of significant modulation anywhere on the Fermi surface. This reinforces the statement made earlier on the basis of thermal conductivity data in Co-Ba122,[20] that superconductivity in pnictides is strongest when isotropic, pointing fundamentally to a state with s-wave symmetry, at least in the high-T_c members of the pnictide family. Secondly, With underdoping, the superconducting gap becomes small in some parts of the Fermi surface. The minimum gap gets weaker and weaker with decreasing x. Because this modulation of the gap appears with the onset of antiferromagnetic order, we attribute it to the associated reconstruction of the Fermi surface. Third, although it acquires minima, the superconducting gap structure of underdoped K-Ba122 never develops nodes, where the gap goes to zero. This is in contrast with underdoped Co-Ba122, whose gap does have nodes.

VI. ACKNOWLEDGEMENTS

We thank A. V. Chubukov, R. M. Fernandes, P. J. Hirschfeld, D.-H. Lee and I. I. Mazin for fruitful discussions and J. Corbin for his assistance with the experiments. The work at Sherbrooke was supported by a Canada Research Chair, the Canadian Institute for Advanced Research, the National Science and Engineering Research Council of Canada, the Fonds de recherche du Québec - Nature et Technologies, and the Canada Foundation for Innovation. The work at the Ames Laboratory was supported by the DOE-Basic Energy Sciences under Contract No. DE-AC02-07CH11358. The work in China was supported by NSFC and the MOST of China (#2011CBA00100). H.S. acknowledges the support of the Iran National Science Foundation.

* E-mail: louis.taillefer@usherbrooke.ca

[1] Y. Kamihara, T. Watanabe, M. Hirano, and H. Hosono, J. Am. Chem. Soc. **130**, 3296 (2008).
[2] L. Boeri, O. V. Dolgov, and A. A. Golubov, Phys. Rev. Lett. **101**, 026403 (2008).
[3] L. Taillefer, Ann. Rev. Cond. Matter Physics **1**, 51 (2010).
[4] P. Monthoux, D. Pines, and G. G. Lonzarich, Nature **450**, 1177 (2007).
[5] M. R. Norman, Science **332**, 196 (2011).
[6] D. J. Scalapino, Rev. Mod. Phys. **84**, 1383 (2012).
[7] I. I. Mazin, D. J. Singh, M. D. Johannes, and M. H. Du, Phys. Rev. Lett. **101**, 057003 (2008).
[8] M. Rotter, M. Tegel, and D. Johrendt, Phys. Rev. Lett. **101**, 107006 (2008).
[9] H. Q. Luo, Z. S. Wang, H. Yang, P. Cheng, X. Zhu, and H.-H. Wen, Supercond. Sci. Technol. **21**, 125014 (2008).
[10] A. S. Sefat, R. Jin, M. A. McGuire, B. C. Sales, D. J. Singh, and D. Mandrus, Phys. Rev. Lett. **101**, 117004 (2008).
[11] P. C. Canfield and S. L. Bud'ko, Ann. Rev. Cond. Mat. Phys. **1**, 27 (2010).
[12] S. Kasahara, T. Shibauchi, K. Hashimoto, K. Ikada, S. Tonegawa, R. Okazaki, H. Shishido, H. Ikeda, H. Takeya, K. Hirata, T. Terashima, and Y. Matsuda, Phys. Rev. B **81**, 184519 (2010).
[13] H. Ding, P. Richard, K. Nakayama, K. Sugawara, T. Arakane, Y. Sekiba, A. Takayama, S. Souma, T. Sato, T.

Takahashi, Z. Wang, X. Dai, Z. Fang, G. F. Chen, J. L. Luo, and N. L. Wang, Europhys. Lett. **83**, 47001 (2008).
[14] I. I. Mazin, Nature **464**, 183 (2010).
[15] K. Hashimoto, K. Cho, T. Shibauchi, S. Kasahara, Y. Mizukami, R. Katsumata, Y. Tsuruhara, T. Terashima, H. Ikeda, M. A. Tanatar, H. Kitano, N. Salovich, R. W. Giannetta, P. Walmsley, A. Carrington, R. Prozorov, Y. Matsuda, Science **336**, 1554 (2012).
[16] X. Qiu, S. Y. Zhou, H. Zhang, B. Y. Pan, X. C. Hong, Y. F. Dai, Man Jin Eom, Jun Sung Kim, Z. R. Ye, Y. Zhang, D. L. Feng, and S. Y. Li, Physical Review X **2**, 011010 (2012)
[17] R. T. Gordon, C. Martin, H. Kim, N. Ni, M. A. Tanatar, J. Schmalian, I. I. Mazin, S. L. Bud'ko, P. C. Canfield, and R. Prozorov Phys. Rev. B **79**, 100506 (R) (2009).
[18] C. Martin, H. Kim, R. T. Gordon, N. Ni, V. G. Kogan, S. L. Bud'ko, P. C. Canfield, M. A. Tanatar, and R. Prozorov, Phys. Rev. B **81**, 060505 (2010).
[19] M.A. Tanatar, J.-Ph. Reid, H. Shakeripour, X. G. Luo, N. Doiron-Leyraud, N. Ni, S. L. Bud'ko, P. C. Canfield, R. Prozorov, and L. Taillefer, Phys. Rev. Lett. **104**, 067002 (2010).
[20] J.-Ph. Reid, M. A. Tanatar, H. Shakeripour, X. G. Luo, N. Doiron-Leyraud, N. Ni, S. L. Bud'ko, P. C. Canfield, R. Prozorov, and L. Taillefer, Phys. Rev. B **82**, 064501 (2010).
[21] K. Gofryk, A. S. Sefat, M. A. McGuire, B. C. Sales, D. Mandrus, J. D. Thompson, E. D. Bauer, and F. Ronning, Phys. Rev. B **81**, 184518 (2010).
[22] J.-Ph. Reid, A. Juneau-Fecteau, R. T. Gordon, S. Rene de Cotret, N. Doiron-Leyraud, X. G. Luo, H. Shakeripour, J. Chang, M. A. Tanatar, H. Kim, R. Prozorov, T. Saito, H. Fukazawa, Y. Kohori, K. Kihou, C. H. Lee, A. Iyo, H. Eisaki, B. Shen, H.-H. Wen, Louis Taillefer, Supercond. Sci. Technol. **25**, 084013 (2012).
[23] X. G. Luo, M. A. Tanatar, J.-Ph. Reid, H. Shakeripour, N. Doiron-Leyraud, N. Ni, S. L. Bud'ko, P. C. Canfield, H. Luo, Z. Wang, H.-H. Wen, R. Prozorov, and L. Taillefer, Phys. Rev. B **80**, 140503 (R) (2009).
[24] C. Martin, R. T. Gordon, M. A. Tanatar, H. Kim, N. Ni, S. L. Bud'ko, P. C. Canfield, H. Luo, H. H. Wen, Z. Wang, A. B. Vorontsov, V. G. Kogan, and R. Prozorov, Phys. Rev. B **80**, 020501(R) (2009).
[25] H. Kim, M. A. Tanatar, W. E. Straszheim, K. Cho, J. Murphy, N. Spyrison, J.-Ph. Reid, Louis Taillefer, Bing Shen, Hai-Hu Wen, R. M. Fernandes, and R. Prozorov, Phys. Rev. B **90**, 014517 (2014).
[26] K. Cho, M. Kończykowski, J. Murphy, H. Kim, M. A. Tanatar, W. E. Straszheim, B. Shen, H. H. Wen, and R. Prozorov Phys. Rev. B **90**, 104514 (2014).
[27] H. Fukazawa, Y. Yamada, K. Kondo, T. Saito, Y. Kohori, K. Kuga, Y. Matsumoto, S. Nakatsuji, H.Kito, P.M. Shirage, K. Kihou, N. Takeshita, C.-H. Lee, A. Iyo, and H. Eisaki, J. Phys. Soc. Jpn. **78**, 033704 (2009).
[28] K. Hashimoto, A. Serafin, S. Tonegawa, R. Katsumata, R. Okazaki, T. Saito, H. Fukazawa, Y. Kohori, K. Kihou, C. H. Lee, A. Iyo, H. Eisaki, H. Ikeda, Y. Matsuda, A. Carrington, and T. Shibauchi, Phys. Rev. B **82**, 014526 (2010).
[29] J. K. Dong, S. Y. Zhou, T. Y. Guan, H. Zhang, Y. F. Dai, X. Qiu, X. F. Wang, Y. He, X. H. Chen, and S. Y. Li, Phys. Rev. Lett. **104**, 087005 (2010).
[30] J.-Ph. Reid, M. A. Tanatar, A. Juneau-Fecteau, R. T. Gordon, S. R. de Cotret, N. Doiron-Leyraud, T. Saito, H. Fukazawa, Y. Kohori, K. Kihou, C. H. Lee, A. Iyo, H. Eisaki, R. Prozorov, and L. Taillefer, Phys. Rev. Lett. **109**, 087001 (2012).
[31] D. Watanabe, T. Yamashita, Y. Kawamoto, S. Kurata, Y. Mizukami, T. Ohta, S. Kasahara, M. Yamashita, T. Saito, H. Fukazawa, Y. Kohori, S. Ishida, K. Kihou, C. H. Lee, A. Iyo, H. Eisaki, A. B. Vorontsov, T. Shibauchi, and Y. Matsuda, Phys. Rev. B **89**, 115112 (2014).
[32] K. Okazaki, Y. Ota, Y. Kotani, W. Malaeb, Y. Ishida, T. Shimojima, T. Kiss, S. Watanabe, C.-T. Chen, K. Kihou, C. H. Lee, A. Iyo, H. Eisaki, T. Saito, H. Fukazawa, Y. Kohori, K. Hashimoto, T. Shibauchi, Y. Matsuda, H. Ikeda, H. Miyahara, R. Arita, A. Chainani, and S. Shin, Science 337, 1314 (2012).
[33] Ronny Thomale, Christian Platt, Werner Hanke, Jiangping Hu, and B. Andrei Bernevig Phys. Rev. Lett. **107**, 117001 (2011).
[34] A. V. Chubukov, Annu. Rev. Cond. Mat. Phys. **3**, 57 (2012).
[35] P. J. Hirschfeld, M. M. Korshunov, and I. I. Mazin, Rep. Prog. Phys. **74**, 124508 (2011)
[36] S. Maiti, R. M. Fernandes, and A. V. Chubukov, Phys. Rev. B **85**, 144527 (2012).
[37] R. T. Gordon, H. Kim, N. Salovich, R. W. Giannetta, R. M. Fernandes, V. G. Kogan, T. Prozorov, S. L. Bud'ko, P. C. Canfield, M. A. Tanatar, and R. Prozorov Phys. Rev. B 82, 054507 (2010).
[38] M. A. Tanatar, W. E. Straszheim, Hyunsoo Kim, J. Murphy, N. Spyrison, E. C. Blomberg, K. Cho, J.-Ph. Reid, Bing Shen, Louis Taillefer, Hai-Hu Wen, R. Prozorov, Phys. Rev. B **89**, 144514 (2014).
[39] M. A. Tanatar, N. Ni, S. L. Bud'ko, P. C. Canfield, and R. Prozorov, Supercond. Sci. Technol. **23**, 054002 (2010).
[40] M. A.Tanatar, R. Prozorov, N. Ni, S. L. Bud'ko, and P. C. Canfield, U.S. Patent 8,450,246.
[41] Y. Liu, M. A. Tanatar, W. E. Straszheim, B. Jensen, K. W. Dennis, R. W. McCallum, V. G. Kogan, R. Prozorov, T. A. Lograsso, Phys. Rev. B **89**, 134504 (2014).
[42] H. Shakeripour, C. Petrovic, and L. Taillefer, New J. Phys. **11**, 055065 (2009).
[43] J. Lowell and J.B. Sousa, J. Low Temp. Phys. **3**, 65 (1970).
[44] E. Boaknin, M. A. Tanatar, J. Paglione, D. G. Hawthorn, F. Ronning, R. W. Hill, M. Sutherland, L. Taillefer, J. Sonier, S. M. Hayden, and J. W. Brill, Phys. Rev. Lett. **90**, 117003 (2003).
[45] C. Proust, E. Boaknin, R.W. Hill, L. Taillefer, and A. P. Mackenzie, Phys. Rev. Lett. **89**, 147003 (2002).
[46] M. Sutherland, D. G. Hawthorn, R. W. Hill, F. Ronning, S. Wakimoto, H. Zhang, C. Proust, E. Boaknin, C. Lupien, L. Taillefer, R. Liang, D. A. Bonn, W. N. Hardy, R. Gagnon, N. E. Hussey, T. Kimura, M. Nohara, and H. Takagi, Phys. Rev. B **67**, 174520 (2003).
[47] S. Y. Li, J.-B. Bonnemaison, A. Payeur, P. Fournier, C. H. Wang, X. H. Chen, and L. Taillefer, Phys. Rev. B **77**, 134501 (2008).
[48] E. Boaknin, R. W. Hill, C. Proust, C. Lupien, L. Taillefer, P. C. Canfield, Phys. Rev. Lett. **87**, 237001 (2001).
[49] A. V. Sologubenko *et al.*, Phys. Rev. B **66**, 014504 (2002).
[50] A. V. Chubukov, M. G. Vavilov, and A. B. Vorontsov, Phys. Rev. B **80**, 140515 (2009).
[51] F. Wang and D.-H.Lee, Phys. Rev. Lett. **102**, 047005 (2009).
[52] S. Graser S. Graser, T. A. Maier, P. J. Hirschfeld, and D. J. Scalapino, New J. Phys. **11**, 025016 (2009).

[53] S. Avci, O. Chmaissem, E. A. Goremychkin, S. Rosenkranz, J.-P. Castellan, D. Y. Chung, I. S. Todorov, J. A. Schlueter, H. Claus, M. G. Kanatzidis, A. Daoud-Aladine, D. Khalyavin, and R. Osborn, Phys. Rev. B **83**, 172503 (2011).

[54] D. Parker, M. G. Vavilov, A. V. Chubukov, and I. I. Mazin Phys. Rev. B **80**, 100508 (2009).

[55] R. M. Fernandes and A. J. Millis, Phys. Rev. Lett. **111**, 127001 (2013).

[56] A. E. Böhmer, F. Hardy, L. Wang, T. Wolf, P. Schweiss and C. Meingast, Nat. Comm. **6**, 7911 (2015).

[57] E. G. Moon and S. Sachdev, Phys. Rev. B **85**, 184511 (2012)).